AD-A284 289

PAGE

Form Approved
OBM No. 0704-0188

Public reporting bur... nse, including the time for reviewing instructions, searching existing data sources, gathering and maintaining the data... nents regarding this burden or any other aspect of this collection of information, including suggestions for reducing this bu... ations and Reports, 1215 Jefferson Davis Highway, Suite 1204, Arlington, VA 22202-4302, and to the Office of Manag... DC 20503.

**1. Agency Use Only** (Leave blank).

1994

**3. Report Type and Dates Covered.**
Final - Journal Article

**4. Title and Subtitle.**
Circle Detection for Extracting Eddy Size and Position from Satellite Imagery of the Ocean

**5. Funding Numbers.**
*Program Element No.* 0602435N
*Project No.* 3582
*Task No.* MOG
*Accession No.* DN256010
*Work Unit No.* 13212R

**6. Author(s).**
Peckinpaugh, S. and R. Holyer

**7. Performing Organization Name(s) and Address(es).**
Naval Research Laboratory
Remote Sensing Applications Branch
Stennis Space Center, MS 39529-5004

**8. Performing Organization Report Number.**
IEEE Trans. on Geoscience & Remote Sensing, Vol. 32, No. 2, March 1994, pp. 267-273

**9. Sponsoring/Monitoring Agency Name(s) and Address(es).**
Naval Research Laboratory
Center for Environmental Acoustics
Stennis Space Center, MS 39529-5004

**10. Sponsoring/Monitoring Agency Report Number.**
NRL/JA:321:065:92

**11. Supplementary Notes.**

**12a. Distribution/Availability Statement.**
Approved for public release; distribution is unlimited.

"Original contains color plates: All DTIC reproductions will be in black and white"

**12b. Distribution Code.**

**13. Abstract** *(Maximum 200 words).*

This paper evaluates the ability of several circle detectors to define the size and position of warm and cold eddies in oceanographic satellite imagery. The Advanced Very High Resolution Radiometer channel 4 (10.3-11.3 μm) or sea surface test images are reduced to binary edge images. Six different circle detectors are then applied to the edge images. The automated results are compared to eddies defined by a trained analyst.

DTIC
ELECTE
SEP 0 9 1994
S D
F

8pg 94-29304
425 300

DTIC QUALITY INSPECTED 3

**14. Subject Terms.**
Remote Sensing; Artificial Intelligence; Data Assimilation; Satellite Data

**15. Number of Pages.**
7

**16. Price Code.**

| 17. Security Classification of Report. | 18. Security Classification of This Page. | 19. Security Classification of Abstract. | 20. Limitation of Abstract. |
|---|---|---|---|
| Unclassified | Unclassified | Unclassified | SAR |

# DISCLAIMER NOTICE

THIS DOCUMENT IS BEST QUALITY AVAILABLE. THE COPY FURNISHED TO DTIC CONTAINED A SIGNIFICANT NUMBER OF COLOR PAGES WHICH DO NOT REPRODUCE LEGIBLY ON BLACK AND WHITE MICROFICHE.

# Circle Detection for Extracting Eddy Size and Position from Satellite Imagery of the Ocean

Sarah H. Peckinpaugh and Ronald J. Holyer

*Abstract*—**This paper evaluates the ability of several circle detectors to define the size and position of warm and cold eddies in oceanographic satellite imagery. The Advanced Very High Resolution Radiometer channel 4 (10.3–11.3 μm) or sea surface temperature test images are reduced to binary edge images. Six different circle detectors are then applied to the edge images. The automated results are compared to eddies defined by a trained analyst.**

## Introduction

INFRARED (IR) images of the ocean obtained from satellite sensors are widely used for the study of ocean dynamics [1]–[6]. Many studies involve analyzing large data sets of IR imagery. It is desirable to replace the labor-intensive time-consuming manual interpretation of IR imagery with automated analysis. And, because of the current worldwide awareness of the effects of climatology and global change, the impetus is now on both speed and accuracy.

Therefore, the Naval Research Laboratory began development of the Semi-Automated Mesoscale Analysis System (SAMAS)—a comprehensive set of algorithms that handles the entire automated analysis problem. The SAMAS performs the low-level edge detection through feature formation and higher level artificial intelligence modules that estimate positions of previously detected features when cloud cover obscures direct observation in the current image set [7]. Feature locations produced automatically by SAMAS compare favorably to human interpretation of the same images [8], [9]. An important part of the SAMAS is the eddy detection based on an ensemble of edge fragments that have been labeled by a feature-labeling module as being part of an eddy [10]. The SAMAS uses the Hough Transform to define eddy position and size. This paper evaluates the effectiveness and compares the results for six methods of circle detection, including the Hough Transform method.

## Preprocessing

The test data consist of 18 IR images of the Gulf Stream area of the North Atlantic Ocean. These images were obtained from the AVHRR sensor aboard a National Oceanic and Atmospheric Administration satellite. Images are calibrated; the channel 4 images are scaled to 8 bits, such that 0 corresponds to 0°C and 255 corresponds to 25.5°C, and are then remapped to a Mercator projection. Each image is 256 × 256 pixels with a warm or cold eddy in the center of the image. Resolution of the test images is about 2.5 km/pixel. From each image, a binary edge image was created.

The method of edge detection used to create the edges is described by Holyer and Peckinpaugh [11], but we modified the zero crossing test slightly. The modification uses a second threshold to extend edges found using the original method. The results of this type of edge detection are 2-pixel-wide lines at the edges. The lines are dilated from 2-pixel-wide edges to 4-pixel-wide edges. An analyst subjectively edited the edges and kept only those considered to be associated with the eddy. A second analyst looked at only the IR images using an interactive editor, and subjectively defined the center coordinates and the radius of the eddies for each image. Fig. 1 shows the test images, the detected edges, and the circle fit subjectively defined by the human expert.

These visually defined center coordinates and radii will be used to evaluate the eddy detection methods. In Fig. 1, darker shades indicate warmer temperatures, red indicates edges, and yellow indicates the analyst-defined eddies. The eddy images selected as test cases are typical of those encountered in a day-to-day operational environment. That is, some have very weak surface expression and others are partly cloud covered. The test has not been biased by inclusion of only ideal test cases. Cold eddies are generally more difficult to observe than warm eddies because the dense, cold water tends to sink quickly, thereby greatly reducing the surface IR signature. The test cases include 10 cold eddies [Fig. 1(a)–(j)] and 8 warm eddies [Fig. 1(k)–(r)].

## Circle Detection

The six algorithms selected for testing are referred to by the following names: Hough, Thomas_Chan, Landau, Albano, Janowitz, and Circle_Fit. Some of these algorithms were modified slightly from the original descriptions to tailor the algorithm better to the input data or to the desired output. The methods as they were used in this study are defined briefly below.

Manuscript received August 14, 1992; revised September 28, 1993. This work was supported by the Office of Naval Research, Program Element 0602435N, Program Manager, Dr. T. Warfield. NRL Contribution 321:065:92.

The authors are with the Naval Research Laboratory, Stennis Space Center, MS 39529-5004.

IEEE Log Number 9215114.

0196/2892/94$04.00 © 1994 IEEE

DTIC QUALITY INSPECTED 3

94 9 07 113

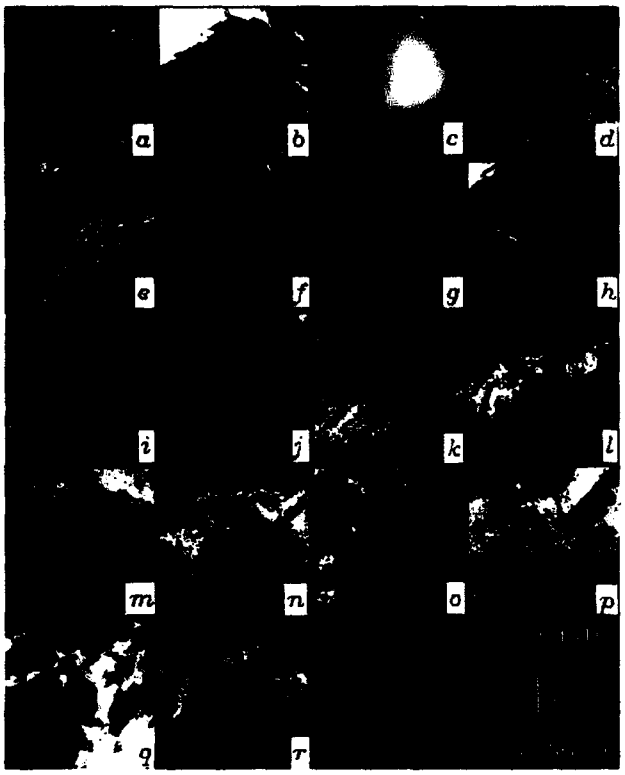


Fig. 1. IR images of eddies. Actual edges are red, and analysis-defined eddies are yellow. (a) Cold eddy, SST image centered at 36.09 latitude −71.18 longitude; Jan. 14, 1987. (b) Cold eddy, SST image centered at 35.89 latitude −70.53 longitude; Mar. 7, 1987. (c) Cold eddy, SST image centered at 36.46 latitude −67.24 longitude; May 11, 1987. (d) Cold eddy, SST image centered at 34.95 latitude −66.29 longitude; June 1, 1987. (e) Cold eddy, SST image centered at 35.69 longitude −68.34 longitude; June 26, 1986. (f) Cold eddy, SST image centered at 35.89 latitude −67.94 longitude; July 8, 1986. (g) Cold eddy, SST image centered at 37.82 latitude −66.69 longitude; July 15, 1986. (h) Cold eddy, SST image centered at 33.75 latitude −71.68 longitude; May 11, 1987. (i) Cold eddy, SST image centered at 36.18 latitude −63.40 longitude; June 11, 1987. (j) Cold eddy, SST image centered at 37.62 latitude −57.66 longitude; May 11, 1987. (k) Warm eddy, Channel 4 image centered at 40.23 latitude −63.55 longitude; Dec. 4, 1986. (l) Warm eddy, SST image centered at 38.88 latitude −70.13 longitude; Mar. 7, 1987. (m) Warm eddy, SST image centered at 40.80 latitude −57.31 longitude; May 11, 1987. (n) Warm eddy, SST image centered at 41.74 latitude −58.31 longitude; June 11, 1987. (o) Warm eddy, SST image centered at 39.46 latitude −68.04 longitude; Sept. 5, 1986. (p) Warm eddy, SST image centered at 39.34 latitude −70.03 longitude; Nov. 17, 1986. (q) Warm eddy, Channel 4 image centered at 39.93 latitude −65.54 longitude; Mar. 25, 1987. (r) Warm eddy, SST image centered at 39.07 latitude −68.04 longitude; Apr. 11, 1987.

### *Hough*

Duda and Hart [12] provide a general description of the circular Hough Transform. The Hough method can be conceptualized as a convolution of various binary kernels, each containing a circle of "1s" of some selected radius, with the binary edge image. If all possible radii are represented in the library of convolution kernels, the kernel resulting in the highest convolution result identifies the best estimate of radius for any circular structure that might be in the edge image. The $x$ and $y$ convolution lag values, where the maximum output occurs, identify the best estimate of center coordinates for the circular structure. This convolution procedure can be shown to be mathematically optimal in the least-mean-squares sense for circles contained as additive signal in a random, uncorrelated noise background. The mathematical optimality may not strictly apply in the present case where circles are represented by scattered edge fragments. However, the detection performance known to result from convolution of an image with a kernel containing the desired target suggests that the Hough Transform method should be investigated.

In practice, the Hough method does not perform the multiple convolutions described. Rather, it performs an equivalent but much more efficient operation, which involves incrementing the elements of an accumulator array for each edge pixel in the edge image. The final accumulator array is then searched for the maximum value. The address of the maximum value in the accumulator array defines center coordinates and the radius of a circle, representing a best fit to the image edge fragments.

For the sake of better computational efficiency, our implementation of the Hough method uses a two-dimensional accumulator rather than a three-dimensional array. The third dimension is avoided by not simultaneously considering all possible radius values, but by considering one radius value at a time. The starting point for radius is the largest geophysically reasonable radius (133 km for this study). Radius is then decremented until a case is reached where a circle is found which has 40% of its circumference occupied by an edge pixel.

Given a set of points defined as $(x_i, y_i)$, $i = 1, 2, \cdots, N$, the Hough Transform is applied as follows.

a) Convert the upper limit of 133 km to a discrete pixel measure, $R_1$.
b) Zero all values of the two-dimensional accumulator array, $A$.
c) Using Bresenham's [13] algorithm, compute the list of discrete coordinates $(x_b, y_b)$ for a circle of radius $R_j$ centered at (0, 0). Also computed is the number of points forming the circle, $N_b$.
d) Increment values of $A$: $A_{x_i + x_b, y_i + y_b} = A_{x_i + x_b, y_i + y_b} + 1$.
e) Select the maximum value from $A$, $A_{xm, ym}$. If $(N_b * 0.4) > A_{xm, ym}$, then $R_{j+1} = R_j - 1$, and go to step b.
f) $X_c = xm$, $Y_c = ym$, and $R = R_j$.

### *Thomas_Chan*

Given a set of points defined as $(x_i, y_i)$, $i = 1, 2, \cdots, N$, Thomas and Chan [14] propose that the center position and radius

$$X_c = \frac{c_1 b_2 - c_2 b_1}{a_1 b_2 - a_2 b_1} \qquad Y_c = \frac{a_1 c_2 - a_2 c_1}{a_1 b_2 - a_2 b_1}$$

can be computed as follows:

$$R^2 = \frac{1}{N}\left(\sum x_i^2 - 2\sum x_i X_c + N X_c^2 + \sum y_i^2 - 2\sum y_i Y_c + N Y_c^2\right)$$

where

$$a_1 = 2\left(\sum x_i^2 - N\sum x_i^2\right)$$

$$b_1 = 2\left(\sum x_i \sum y_i - N\sum x_i y_i\right)$$

$$a_2 = 2\left(\sum x_i \sum y_i - N\sum x_i y_i\right) = b_1$$

$$b_2 = 2\left(\sum x_i^2 - N\sum y_i^2\right)$$

$$c_1 = \left(\sum x_i^2 \sum x_i - N\sum x_i^3 + \sum x_i \sum y_i^2 - N\sum x_i y_i^2\right)$$

$$c_2 = \left(\sum x_i^2 \sum y_i - N\sum y_i^3 + \sum y_i \sum y_i^2 - N\sum x_i^2 y_i\right)$$

These equations result from minimization of a theoretical error function in $X_c$, $Y_c$, and $R$. The reader is referred to the original paper for the definition of the area-based error function and the mathematics of minimization leading to the equations listed here.

*Landau*

Given a set of points defined as $(x_i, y_i)$, $i = 1, 2, \cdots, N$, Landau [15] suggests an iterative method for computing the center position and radius. The algorithm is applied to the data as follows.

a) For $\bar{a} = (X_c, Y_c)$, the center coordinates of the circle, initialize $\bar{a}_0 = (X_a, Y_a)$, where

$$X_a = \frac{1}{N}\sum x_i \qquad Y_a = \frac{1}{N}\sum y_i.$$

b) Use $\bar{a}_k$ to compute the associated radius $R_k$

$$R_k = \frac{1}{N}\sum |\bar{r}_i - \bar{a}_k|$$

where $\bar{r}_i = (x_i, y_i)$.

c) Use $\bar{a}_k$ and $R_k$ to compute $\bar{a}_{k+1}$

$$\bar{a}_{k+1} = \frac{1}{N}\sum (\bar{r}_i - R_k \bar{1}_{r_i - a_k}).$$

d) If $|\bar{a} - \bar{a}_{k+1}| > 0.000001$, then go to step b.

This method also involves minimization of an error function, which is the LMS distance from the set of data points to the circle defined by $X_c$, $Y_c$, and $R$. Minimization of the LMS error function does not lead to an exact solution, thus the need for the iterative approach.

*Albano*

Albano [16] suggests solving the following general conic equation:

$$Ax^2 + Bxy + Cy^2 + Dx + Ey + 1.0 = 0$$

to fit conic sections to edge points.

This method is more general than the others in that it can be used to fit any conic arc, not just circles, to the data. However, we have constrained the solution here to provide only circular fits. The method employs least-squares minimization of the conic equation evaluated at all data points. Coordinate standardization [16] is also performed in conjunction with this method.

The steps to compute the center coordinates $(X_c, Y_c)$ and radius $R$ are as follows.

a) Coordinate standardization:

$$X_b = \frac{1}{N}\sum x_i \qquad Y_b = \frac{1}{N}\sum y_i$$

$$\bar{x}_i = (x_i - X_b) \qquad \bar{y}_i = (y_i - Y_b)$$

$$S = \sqrt{\sum \bar{x}_i + \sum \bar{y}_i}$$

$$x_{si} = \frac{\bar{x}_i}{S} \qquad y_{si} = \frac{\bar{Y}_i}{S}.$$

b) Solve the following simultaneous linear equations for $A$, $B$, $C$, $D$, and $E$:

$$A\sum x_{si}^4 + B\sum x_{si}^3 y_{si} + C\sum x_{si}^2 y_{si}^2 + D\sum x_{si}^3 + E\sum x_{si}^2 y_{si} + \sum x_{si}^2 = 0$$

$$A\sum x_{si}^3 y_{si} + B\sum x_{si}^2 y_{si}^2 + C\sum x_{si} y_{si}^3 + D\sum x_{si}^2 y_{si} + E\sum x_{si} y_{si}^2 + \sum x_{si} y_{si} = 0$$

$$A\sum x_{si}^2 y_{si}^2 + B\sum x_{si} y_{si}^3 + C\sum y_{si}^4 + D\sum x_{si} y_{si}^2 + E\sum y_{si}^3 + \sum y_{si}^2 = 0$$

$$A\sum x_{si}^3 + B\sum x_{si}^2 y_{si} + C\sum x_{si} y_{si}^2 + D\sum x_{si}^2 + E\sum x_{si} y_{si} + \sum y_{si} = 0$$

$$A\sum x_{si}^2 y_{si} + B\sum x_{si} y_{si}^2 + C\sum y_{si}^3 + D\sum x_{si} y_{si} + E\sum y_{si}^2 + \sum y_{si} = 0.$$

c) Compute the center coordinates:

$$X_c = \left(\frac{2CD - BE}{B^2 - 4AC}\right) S + X_b$$

$$Y_c = \left(\frac{2AE - BD}{B^2 - 4AC}\right) S + Y_b.$$

d) Compute the radius for a circle:

$$R = \frac{\sum \sqrt{(X_c - x_i)^2 + (Y_c - y_i)^2}}{N}.$$

*Janowitz*

The Janowitz method has been modified from an ellipse detection scheme [4] to a circle detection scheme. Janowitz also did a proximity test of edge pixels to a candidate center pixel position. If an edge pixel was determined to be close to the candidate center pixel position, then that position was no longer considered a candidate. This test did not work well with these edges and was omitted.

This algorithm shoots rays in 52 directions from each candidate center point and records the distance along the ray to the first encounter of an edge pixel. The sum of the distances between the candidate circle and these ray distances is calculated, and the minimum value found indicates the best fit. Since the method considers only the first edge point encountered along each ray, one would expect the Janowitz method to be biased toward smaller radius values.

Given a binary edge image defined as $f(x, y)$, the center coordinates $(X_c, Y_c)$ and radius $R$ are computed as follows.

a) Apply edge thinning algorithm to the image, $f(x, y)$ [17].
b) Initialize variables

$$X_0 = X_c = X_{cm}$$

$$Y_0 = Y_c = Y_{cm}$$

$$\text{MinErr} = 9999.0$$

where $x_{cm}$, $y_{cm}$ are the first possible coordinates of the image $f(x, y)$ that can be considered as a possible center coordinate.

c) Given the set of 52 evenly incremented rays emanating from the center image coordinates $X_0$, $Y_0$ to the outer edge of the window centered about that point, find the distances $d_i$ ($j = 1, 2, \cdots, 52$) from the window center to the first edge pixel, if it exists, located along the ray.
d) MinRad = MIN(33, $d_1, d_2, \cdots, d_{52}$) and MaxRad = MAX(33, $d_1, d_2, \cdots, d_{52}$). Compute the error statistic for each radius between the limits

$$E_m = \frac{\sum |(d_j - m)|}{c},$$

$$m = \text{MinRad}, \cdots, \text{MaxRad},$$

where only those $d_j$ values are used for which an edge pixel was encountered along the ray and within the window, and $c$ is the count of those $d_j$ values actually used to compute the statistic. If ($c < (0.4 * 52)$), then $E_m = 9999.0$.
e) If (MIN($E_{\text{MinRad}}, \cdots, E_{\text{MaxRad}}$) < MinErr), then

$$\text{MinErr} = \text{MIN}(E_{\text{MinRad}}, \cdots, E_{\text{MaxRad}})$$

$$X_c = X_0$$

$$Y_c = Y_0$$

$R$ = radius associated with the new MinErr.

f) If $X_0$, $Y_0$ are not the last possible center coordinates within the image $f(x, y)$, then get next $X_0$, $Y_0$, and go to step c.

*Circle_Fit*

Circle_Fit used the mean (centroid) of the edge points as the circle center, and the mean distance of the points from the center as the radius. Given a set of points defined $(x_i, y_i)$, $i = 1, 2, \cdots, N$, the center coordinates $(X_c, Y_c)$ and the radius $R$ are computed as follows:

$$X_c = \frac{1}{N} \sum x_i \qquad Y_c = \frac{1}{N} \sum y_i$$

$$R = \frac{\sum \sqrt{(X_c - x_i)^2 + (Y_c - y_i)^2}}{N}.$$

## Experimental Results

Figs. 2 and 3 are the results of the six methods applied to the 18 test images. Some methods produced no valid definition for some of the eddies. These no-definition cases are not used for the analysis of that method. The results of the automated methods are compared to the analyst's definition of the eddy.

For each eddy, errors in center position and radius, relative to human judgment, were calculated for each of the circle-detection methods. The circle-detection methods were then compared, pairwise, based on the mean position and radius errors. The statistical validity of the comparison was established using a T-test [18]. The T-test used 18 samples (or less, in the cases having no-definition for an eddy) and two treatments. The results of the comparisons are shown in Tables I and II, where the best method is shown for each pairwise comparison. In all cases, the T-test showed that the differences in the mean error were significant at the 95% confidence level or higher.

*Center Errors*

Notice in Fig. 1 that eddy (c) has a particularly noncircular shape. For all methods except Janowitz, this caused a spike in the graph even if it was not the largest spike for all methods. This would be expected for detection of a noncircular feature using a circle-detection method. There seems to be no trend for better detection of cold over warm or vice versa. Of the method tested, Janowitz is the most erratic. The existence of center structure and large missed edges cause problems. Each method was compared to the others using a T-test to determine statistical significance of the result. This comparison (Table I) shows Thomas_Chan to be the best performing of the methods, Albano is second, and the simple Circle_Fit method is third, leaving Hough, Janowitz, and Albano as the least effective.

*Radius Errors*

Fig. 3 shows the results of each method. Albano and Circle_Fit show trends toward defining larger than analyst

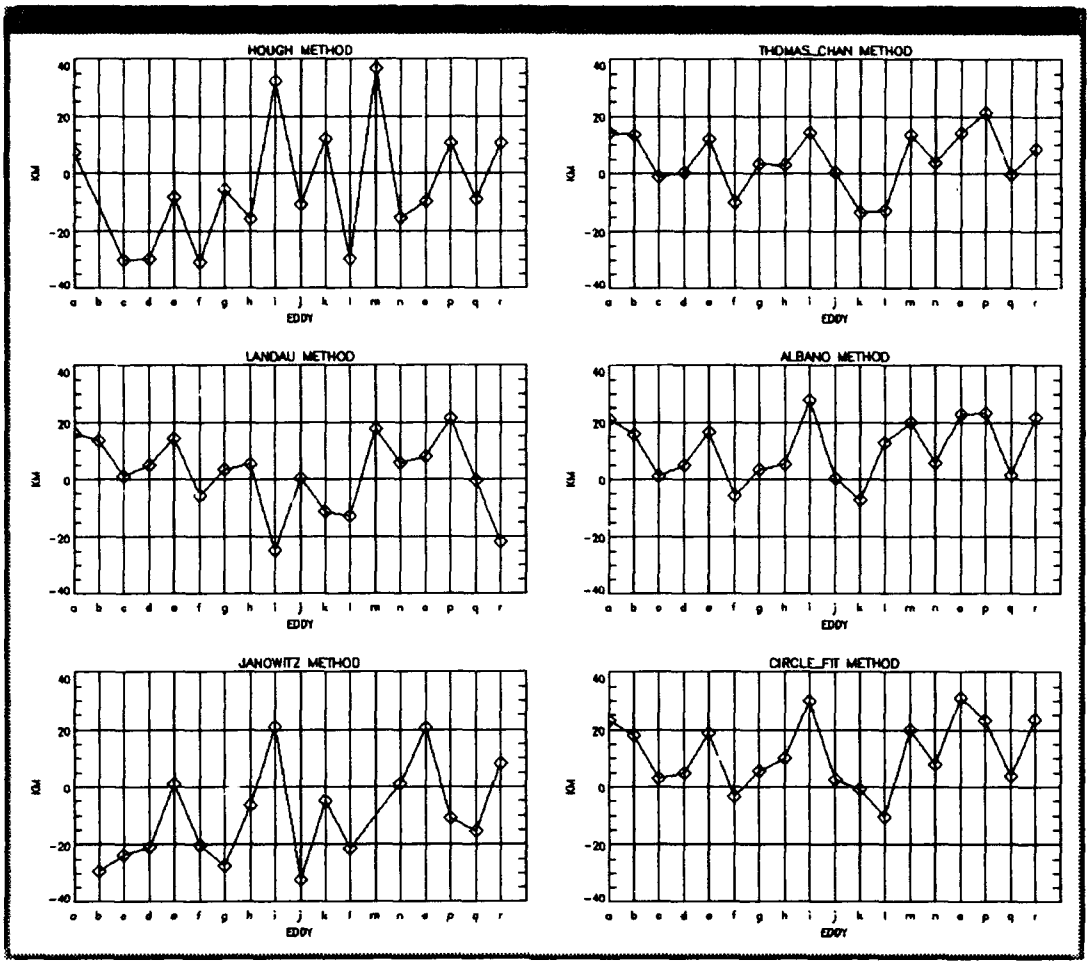


Fig. 2. The six methods are compared for center position with the analyst definition of the 18 eddies (a)–(r).

radius parameters. These trends do not appear to be well defined enough to apply a correction. Hough and Janowitz seem to be the most erratic. Again, the methods are compared using a T-test (Table II). Again, Thomas_Chan performed best, with Landau second, and Albano third. Hough, Janowitz, and Circle_Fit are least effective. There would be no problem defining center position and radius by two different methods, but the results show Thomas_Chan to perform best for each. The eddies used for this study show a wide range of characteristics—center structure, missing outer structure, noncircularity, warm core, and cold core. The data set is small, but some methods have been shown to fail even on this limited data set.

## Conclusions

The Thomas_Chan, Landau, and Albano methods, which are based on mathematical minimization of some error function, tend to produce the best circle fits. The nonmathematically derived methods of Hough, Janowitz, and Circle_Fit tend toward poorer results. This result is not necessarily expected. Certainly, mathematically optimized algorithms will, by definition, give the best mathematical fit to the detected edge fragments. However, it does not necessarily follow that the optimal fit to the fragments will in fact also be the best approximation to the judgment of a human analyst in marking eddies in the image. Yet, in this study, the mathematically based algorithms also most closely matched the subjective human result.

In this study, the Thomas_Chan method produced the best error statistics for both center position and radius. However, we used average error for comparing methods. Had we used another error metric (rms error, for example) one of the other methods might have been the best. Also, circle-fit results will depend on the edge detection that precedes the circle-finding algorithm. Our edge detector is typical, but if another edge detector had been used, the ranking of the methods might have changed. We also had only 18 eddies in our data set. A larger or different data set could have produced slightly different results. For these reasons, it is not possible to definitively select a best circle-fit algorithm based on the results of this study. We can conclude that the mathematically based class of circle detectors does show better agreement with human judgment, even when the machine algorithm is presented with only fragmented and corrupted pieces of the circle, than do such ad hoc algorithms as Hough, Janowitz, and

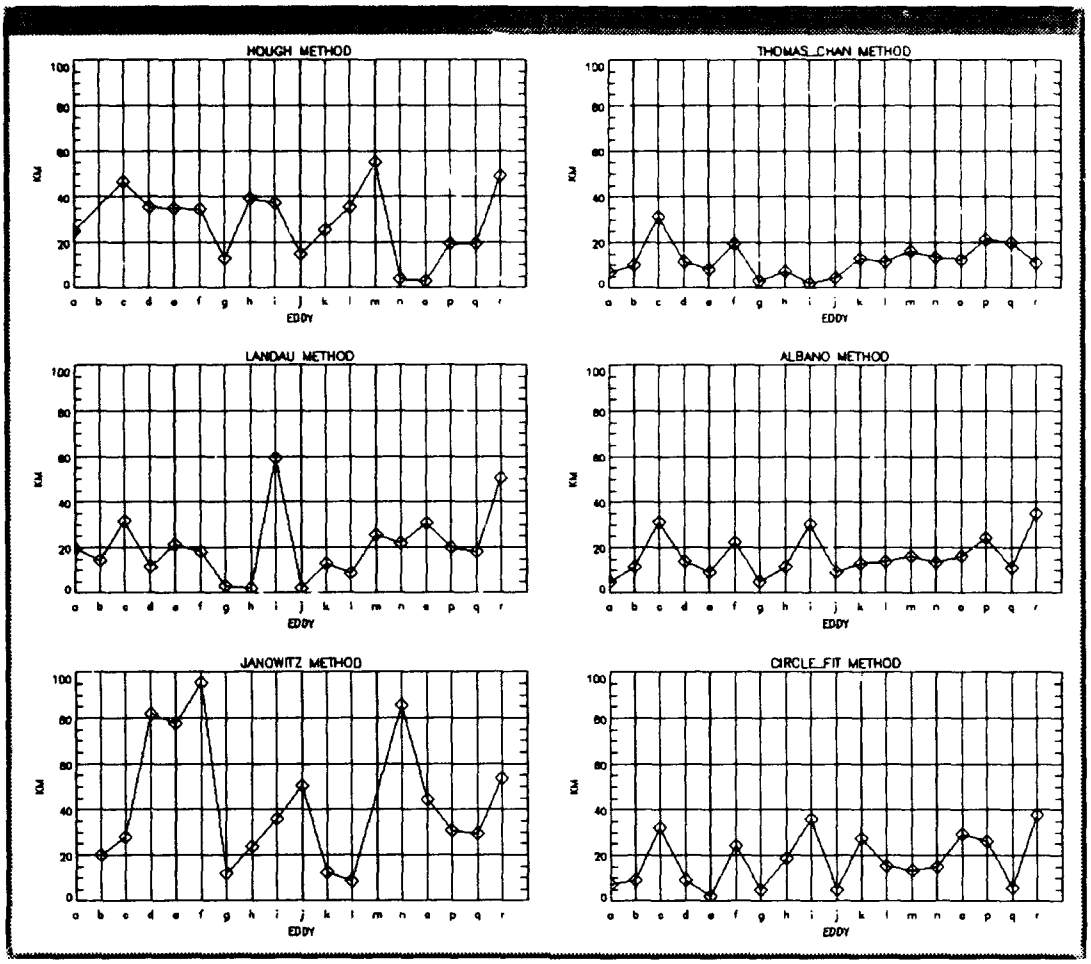


Fig. 3. The six methods are compared for radius with the analyst definition for the 18 eddies (a)–(r).

TABLE I
BEST METHODS DEFINED BY T-TEST FOR CENTER POSITION

| Method 1 → / Method 2 ↓ | HOUGH | THOMAS_CHAN | LANDAU | ALBANO | JANOWITZ | CIRCLE_FIT |
|---|---|---|---|---|---|---|
| HOUGH | | THOMAS_CHAN | LANDAU | ALBANO | HOUGH | CIRCLE_FIT |
| THOMAS_CHAN | THOMAS_CHAN | | THOMAS_CHAN | THOMAS_CHAN | THOMAS_CHAN | THOMAS_CHAN |
| LANDAU | LANDAU | THOMAS_CHAN | | ALBANO | LANDAU | CIRCLE_FIT |
| ALBANO | ALBANO | THOMAS_CHAN | ALBANO | | ALBANO | ALBANO |
| JANOWITZ | HOUGH | THOMAS_CHAN | LANDAU | ALBANO | | CIRCLE_FIT |
| CIRCLE_FIT | CIRCLE_FIT | THOMAS_CHAN | CIRCLE_FIT | ALBANO | CIRCLE_FIT | |

TABLE II
BEST METHODS DEFINED BY T-TEST FOR RADIUS DEFINITION

| Method 1 → / Method 2 ↓ | HOUGH | THOMAS_CHAN | LANDAU | ALBANO | JANOWITZ | CIRCLE_FIT |
|---|---|---|---|---|---|---|
| HOUGH | | THOMAS_CHAN | LANDAU | ALBANO | JANOWITZ | CIRCLE_FIT |
| THOMAS_CHAN | THOMAS_CHAN | | THOMAS_CHAN | THOMAS_CHAN | THOMAS_CHAN | THOMAS_CHAN |
| LANDAU | LANDAU | THOMAS_CHAN | | LANDAU | LANDAU | LANDAU |
| ALBANO | ALBANO | THOMAS_CHAN | LANDAU | | ALBANO | ALBANO |
| JANOWITZ | JANOWITZ | THOMAS_CHAN | LANDAU | ALBANO | | CIRCLE_FIT |
| CIRCLE_FIT | CIRCLE_FIT | THOMAS_CHAN | LANDAU | ALBANO | CIRCLE_FIT | |

Circle_Fit. We conclude that the Hough circle detector that v incorporated into SAMAS without quantitative evaluation was not the best choice.

The circle-fit accuracy in this study was approximately the same for warm and cold eddies. This result was a surprise, since cold eddies offer much fainter thermal signatures than warm eddies. We expected that the weak edge gradients associated with cold eddies would result in poor edge detection, which would in turn introduce errors into the circle fitting. This expectation was not borne out in the present data.

The mean position error is 11.96 km, and the mean radius error is 8.88 km for the Thomas_Chan method. These error values provide a first estimate of the best accuracy with which ocean eddies can be automatically mapped for IR satellite imagery.

## References


[1] D. J. Gerson and P. Gaborski, "Pattern analysis for automatic location of oceanic fronts in digital satellite imagery," Naval Oceanographic Office, Stennis Space Center, MS, TN 3700-65-77, Oct. 1977.

[2] D. J. Gerson, E. Khedouri, and P. Gaborski, "Detecting the Gulf Stream from digital infrared data pattern recognition," in *Belle W. Baruch Library in Marine Science: No. 12—Processes in Marine Remote Sensing*. Columbia, SC: University South Carolina Press, 1982, pp. 19-39.

[3] R. E. Coulter, "Applications of the Bayes decision rule for automatic water mass classification from satellite infrared data," in *Proc. 17th Int. Symp. Remote Sensing Environ.*, vol. II, pp. 589-597, 1983.

[4] M. F. Janowitz, "Automatic detection of Gulf Stream rings," Office Naval Res., Tech. Rep. TR-J8501, Contr. N-000014-79-C-0629, June 1985.

[5] D. G. Nichol, "Autonomous extraction of an eddy-like structure from infrared images of the ocean," *IEEE Trans. Geosci. Remote Sensing*, vol. GE-25, pp. 28-34, 1987.

[6] J. F. Cayula and P. Cornillon, "Edge detection algorithm for SST fields," in *Proc. Digital Image Processing Visual Commun. Technol. Earth Atmospheric Sci.*, SPIE vol. 1301, Apr. 1990, pp. 13-24.

[7] M. Lybanon, S. Peckinpaugh, R. Holyer, and V. Cambridge, "Integrated oceanographic image understanding system," in *Proc. Image Understanding '90s: Building Syst. that Work*, SPIE vol. 1406, 1990, pp. 180-189.

[8] R. J. Holyer and S. H. Peckinpaugh, "Evaluation of the Navy's semi-automated mesoscale analysis system (SAMAS)," in *Proc. 5th Conf. Satellite Meteorol. Oceanogr.*, Boston, MA Amer. Meteorol. Soc., Sept. 1990, pp. 202-207.

[9] S. H. Peckinpaugh and R. J. Holyer, "Evaluation of the Navy's semi-automated mesoscale analysis system (SAMAS)," in *Proc. Automated Interpretation Oceanogr. Satellite Images Workshop*, Naval Res. Lab., Stennis Space Center, MS, SP 001:321:91, Feb. 1991, pp. 57-69.

[10] N. Krishnakumar, S. Iyengar, R. Holyer, and M. Lybanon, "Feature labelling in infrared oceanographic images," *Image Vis. Comput.*, vol. 8, no. 2, pp. 142-147, 1990.

[11] R. J. Holyer and S. H. Peckinpaugh, "Edge detection applied to satellite imagery of the oceans," *IEEE Trans. Geosci. Remote Sensing*, vol. 27, pp. 46-56, Jan. 1989.

[12] R. O. Duda and P. E. Hart, "Use of the Hough transformation to detect lines and curves in pictures," *Commun. ACM*, vol. 15, no. 1, pp. 11-15, Jan. 1972.

[13] J. D. Foley and A. Van Dam, *Fundamentals of Interactive Computer Graphics*. Reading, MA: Addison-Wesley, 1984, pp. 442-444.

[14] S. M. Thomas and Y. T. Chan, "A simple approach for the estimation of circular arc center and its radius," *Comput. Vis., Graph., Image Processing*, vol. 45, no. 3, pp. 362-370, Mar. 1989.

[15] U. M. Landau, "Estimation of a circular arc center and its radius," *Comput. Vis., Graph., Image Processing*, vol. 38, no. 3, pp. 317-326, June 1987.

[16] A. Albano, "Representation of digitized contours in terms of conic arcs and straight-line segments," *Comput. Graph. Image Processing*, vol. 3, pp. 23-33, 1974.

[17] T. Pavlidis, "A thinning algorithm for discrete binary images," *Comput. Graph. Image Processing*, vol. 13, pp. 142-157, 1980.

[18] L. Ott, *An Introduction to Statistical Methods and Data Analysis*. North Scituate, MA: Duxbury, 1977, pp. 250-252, 659.

**Sarah H. Peckinpaugh** received the B.S. degree in computer science with a minor in mathematics from the University of Southern Mississippi in 1981.

She is currently employed at the Naval Research Laboratory, Stennis Space Center, MS. Her current research interests are image segmentation and classification applied to remotely sensed oceanographic data.

**Ronald J. Holyer** received the B.A. degree in physics and mathematics from Augustana College in 1964, the M.S. degree in physics from the South Dakota School of Mines and Technology in 1966, and the Ph.D. degree in geology from the University of South Carolina in 1989.

He has conducted remote-sensing and image-processing research at Texas Instruments, Inc., and Lockheed Electronics Co. He is presently with the Naval Research Laboratory, Stennis Space Center, MS, where he is a Principal Investigator in the field of automated image analysis and pattern recognition techniques.



Accesion For

NTIS CRA&I ☑
DTIC TAB ☐
Unannounced ☐
Justification

By
Distribution /

Availability Codes

| Dist | Avail and / or Special |
|---|---|
| A-1 | 20 |